

Blazar classification from multi-wavelength data using Deep Learning

SAQLAIN AFROZ ,¹ TITIR MUKHERJEE ,² AND RAJ PRINCE ,³

¹ Indian Institute of Science Education and Research Kolkata-741246, India

² Clemson University, Clemson-29634, U.S.A.

³ Department of Physics, Institute of Science, Banaras Hindu University, Varanasi-221005, India

ABSTRACT

The launch of the Fermi-LAT telescope has revolutionized gamma-ray astronomy by detecting over 7,000 gamma-ray emitting objects. A major fraction of the objects are blazars of known type, and a similar fraction of objects were classified as blazars of uncertain types (BCUs). Apart from that, some of the objects were found to be unassociated with any other classes, and no information is available in other wavebands. These types of objects are classified as unassociated objects in the Fermi catalog. To classify the unassociated objects into known categories and BCUs into a known type of blazar, numerous efforts have been made using the machine learning approach. The ideal way of classification would be to have multi-wavelength temporal and spectral information, which is nearly impossible to have for this number of objects in the near future. In this paper, we focus on classifying BCUs into other types of blazars, such as FSRQs and BL Lacs. For this purpose, we have developed for the first time a deep feed-forward Artificial Neural Network (ANN) to classify them, using multi-wavelength data. The complete understanding of blazars can only be known through multi-wavelength observation, and hence, we begin with four input parameters that cover broadband information (radio, optical, X-ray fluxes, and redshift) to train the neural network, and then extend the framework by including additional parameters to examine their impact on the outcome.

Keywords: Galaxies (573) — Active galaxies (17) — Blazars (164) — Gamma-ray astronomy (632) — X-ray astronomy (1810) — Radio astronomy (1338) — Relativistic jets (1390) — Active galactic nuclei (16)

1. INTRODUCTION

Blazars are a subset of AGNs or Active Galactic Nuclei, which are the most luminous extragalactic γ -ray phenomena. Their Spectral Energy Distribution (SED) is bimodal in shape and spans $\log \nu - \log \nu F_\nu$ space over the entire electromagnetic spectrum, from radio to γ -ray band. Their spectral energy is dominated by non-thermal emissions, which are believed to be relativistic in origin. The lower part of this distribution is attributed to synchrotron emission, which is produced by non-thermal electrons moving in the jet magnetic field. The higher energy part is mostly attributed to Inverse Compton scattering of low-energy photons by the relativistic electrons. Blazars can be classified on the basis of the absence or presence of weak emission lines in their optical spectra. BL Lacertae objects (or

BL Lacs) are the ones that have weak or no emission lines, while Flat Spectrum Radio Quasars (or FSRQs) are the ones that have strong emission lines. Another way to classify blazars into BL Lac and FSRQ is based on broadband spectral energy distribution. They differ very much in total jet power and the location of the synchrotron peak in their SED (G. Fossati et al. 1998). One of the properties of these objects is that they are gamma-ray bright and, hence, after the launch of the Fermi LAT telescopes, their number has grown significantly. In the published Fermi catalogs, a bunch of blazars have also been reported, which do not fit into one of the established blazar subtypes, such as BL Lacs or FSRQ. These objects are labeled as BCUs or Blazars of Class Uncertain type. One of the possible reasons is that they lack the optical spectra in the literature, as well as the broadband monitoring or identification of counterparts in different wavebands, which prevents us from creating their broadband SED. The lack of broadband information is mostly influenced by the fact that the

current all-sky monitoring telescopes have poor source localization accuracy (e.g., up to several arcminutes for Fermi-LAT), which yields several potential counterparts and makes the association ambiguous. Since blazars are known for broadband emission, and the physical processes involved can be known only by studying them, it has become essential to have the broadband information for blazar classification.

Since Fermi's first catalog (1FGL) to the fourth catalog (4FGL), we have observed a significant increase in the percentage of BCU objects, from 14% to 42%, it is difficult to have the optical spectra as well as the broadband SED for these objects and hence necessitating the development of algorithms that can efficiently and quickly classify objects into either BL Lacs or FSRQs. This will not only help in classification, but it will also be used to substantiate the extragalactic background light absorption of high-energy photons that will be strategic in the next Cherenkov Telescope Array (CTA) extragalactic survey, which will investigate the physics of high-energy emission from relativistic jets.

The majority of the machine learning approaches used for the source classification are based on the gamma-ray data alone to identify the blazars in the AGN population, or classifying blazars of uncertain type into FSRQs and BL Lacs (S.-J. Kang et al. 2019; M. Kovačević et al. 2020). Some efforts have been made to include the multi-wavelength properties in the process of classifying blazars (A. Kaur et al. 2019; R. de Menezes et al. 2020).

We are taking motivation from works done by: S.-J. Kang et al. (2019) applied three machine learning algorithms, Support Vector Machine, Artificial Neural Network, and Random Forest, to classify 1312 blazar candidates of uncertain type (BCUs) from the Fermi 4FGL catalogue. Using 23 gamma-ray parameters, they achieved up to 92.9% classification accuracy, identifying 724 BL Lacs and 332 FSRQs. Their findings emphasized that feature selection plays a critical role, as incorporating more features does not necessarily enhance performance.

M. Kovačević et al. (2020) utilized artificial neural networks to classify BCUs from the Fermi LAT 8-year source catalogue, focusing on gamma-ray light curves and spectral information. Achieving a precision of 90%, they provided a fast classification method suitable for preliminary analysis when optical data is unavailable, assigning 801 sources as BL Lacs and 406 as FSRQs.

A. Butter et al. (2022) introduced Bayesian neural networks (BNNs) for blazar classification, offering probabilistic uncertainty alongside classification decisions. Their method proved effective on small and imbalanced datasets, and they demonstrated the model's potential

for population studies and guiding observational follow-ups. The inclusion of data augmentation further improved robustness compared to standard dense neural networks.

A. Agarwal (2023) presented a unanimous voting approach across five machine learning algorithms—Random Forest, Logistic Regression, XGBoost, CatBoost, and Neural Networks—to classify 1115 BCUs in the Fermi 4LAC-DR3 catalogue. This ensemble method improved confidence in predictions, classifying 610 sources as BL Lacs and 333 as FSRQs, with an area under the curve (AUC) of 0.96. The study recommended future incorporation of multiwavelength features for improved reliability.

G. Bhatta et al. (2024) employed advanced initialization strategies and self-supervised learning to build a lightweight machine learning framework for classifying Fermi-LAT blazars. Their method emphasized minimal feature reliance and model portability, achieving 93% accuracy while classifying 820 sources as BL Lacs and 295 as FSRQs. The work contributed significantly toward deployable models for astrophysical catalogs.

S. Gharat et al. (2024) extended the classification framework by introducing a multi-task architecture that simultaneously performs blazar classification and redshift estimation. Leveraging traditional neural networks augmented with bias-aware initialization and self-supervised pre-training, their model enhanced reliability and scalability for analyzing gamma-ray active galactic nuclei (AGNs) on a catalogue-wide basis.

In this particular work, we have used a deep neural network approach, which has not been done before, to classify blazars that are from the BCU class into BL Lacs or FSRQs, using multiwavelength data, which helps in providing more diverse features of Blazars. This paper is divided into following sections: Section 2 gives an overview of the data collection and strategy we used to combine them together, as well as a description of our neural network model and training methodology; in section 3 we discuss the results, and finally, in section 4 we summarise the paper in conclusion.

2. DATA COLLECTION AND METHODOLOGY

We utilized multiwavelength data from several authoritative astronomical catalogs to classify and analyze blazars. Specifically, our study integrates data from the Fermi-LAT Fourth Source catalogue (4FGL-DR4) (J. Ballet et al. 2023), the ROMA-BZCAT v5 catalogue (E. Massaro et al. 2015), and the Third LAT AGN catalogue (3LAC) (M. Ackermann et al. 2015). These catalogs collectively provide coverage across the radio, optical, X-ray, and gamma-ray bands, offering a comprehensive

foundation for identifying and distinguishing blazar subclasses.

The 4FGL-DR4 catalogue (J. Ballet et al. 2023) contains gamma-ray observations of active galactic nuclei collected over a span of 14 years. The ROMA-BZCAT v5 (E. Massaro et al. 2015) catalogue includes optically confirmed classifications of blazars, notably BL Lacertae objects (BL Lacs) and flat-spectrum radio quasars (FSRQs). The 3LAC catalogue (M. Ackermann et al. 2015) supplements this information with additional parameters such as synchrotron peak frequencies, spectral types, and power-law indices, which are valuable for refining the classification process.

To create consistent datasets, we performed coordinate-based cross-matching using Right Ascension (RA) and Declination (DEC), applying a positional tolerance of 10 arcseconds. This was implemented using the TOPCAT software (M. Taylor 2017). Two primary datasets were constructed through this process. The first dataset was obtained by cross-matching ROMA-BZCAT v5 with the 4FGL catalogue, resulting in 1,765 matched sources. The second dataset was constructed by matching ROMA-BZCAT v5 with the 3LAC catalogue, producing 1,142 matched sources and incorporating a broader range of features.

For Dataset 1, we selected features that are commonly used in blazar studies and that capture diverse emission mechanisms. These include the radio flux at 1.4 GHz (FR), optical magnitude in the R band (Rmag), X-ray flux in the 0.1–2.4 keV range (FX), and redshift (z). Dataset 2 includes all these features and, in addition, incorporates synchrotron peak frequency, spectral index (gamma-ray spectral index assuming the default spectral type of the source), and power-law index (gamma-ray spectral index assuming a power-law spectrum), thereby offering more detailed spectral information.

These features span across multiple wavelength regimes and represent different physical processes associated with blazar activity. Their inclusion enables a more nuanced understanding of the properties and separability of blazar subclasses within a machine learning framework.

2.1. Implementation and Training of ANN Model

To perform classification on feature vectors derived from observational and simulated datasets, we developed a feedforward Artificial Neural Network (ANN) using the PyTorch framework (A. Paszke et al. 2019). The model was implemented within the `nn.Module` class and encapsulated in a custom module, designed for flexibility and interpretability across different datasets.

The architecture accepts an input feature vector of dimension 4 or 7, which is processed through a sequence of fully connected layers interleaved with non-linear activations. Specifically, the input is first mapped to a hidden representation of size 16, followed by a Rectified Linear Unit (ReLU) activation. This representation is then compressed to 8 dimensions with another ReLU activation, before being mapped to a final 2-dimensional output corresponding to the target classes. A schematic representation of the network is shown in Figure 1.

For training, we employed the Cross-Entropy Loss function (A. Mao et al. 2023), which is well-suited for binary and multi-class classification tasks. Optimization was carried out using the AdamW optimizer (D. P. Kingma & J. Ba 2017) with a learning rate of 1×10^{-4} and a weight decay of 1×10^{-5} to improve generalization. Additionally, a StepLR scheduler was used to decay the learning rate by a factor of 0.1 every 50 epochs, ensuring stable convergence during long training runs.

The training pipeline was constructed using PyTorch’s `DataLoader` utility, with mini-batches of size 32. Instead of relying on a single train–test split, we implemented a 5-fold cross-validation strategy to ensure robust performance assessment and to reduce variance arising from data partitioning J. M. Gorri et al. (2024). For each fold, 80% of the data from both Dataset 1 and Dataset 2 was used for training, while the remaining 20% served as the validation set. The model was trained for 700 epochs in every fold, with mini-batch updates applied throughout each epoch. After each epoch, evaluation was performed on the corresponding validation subset to monitor generalization performance. Key metrics, including training and validation loss, were logged every 10 epochs, and class predictions were obtained by applying the `argmax` operation to the model outputs.

This architecture reflects a careful design trade-off: it is simple enough to mitigate overfitting in domains characterized by limited labeled data or observational noise, yet expressive enough to capture meaningful feature interactions. Moreover, the modular structure of the model makes it straightforward to extend or integrate with more advanced deep learning components—such as convolutional or recurrent layers—should future applications require greater representational capacity.

3. RESULTS AND DISCUSSIONS

The training set was constructed by cross-matching ROMA-BZCAT with 4FGL-DR4 and 3LAC, ensuring that each source had a reliable label as either a BL Lac or an FSRQ. Once trained, the ANN effectively learns the mapping between these multi-wavelength features and the two blazar classes, allowing direct application to

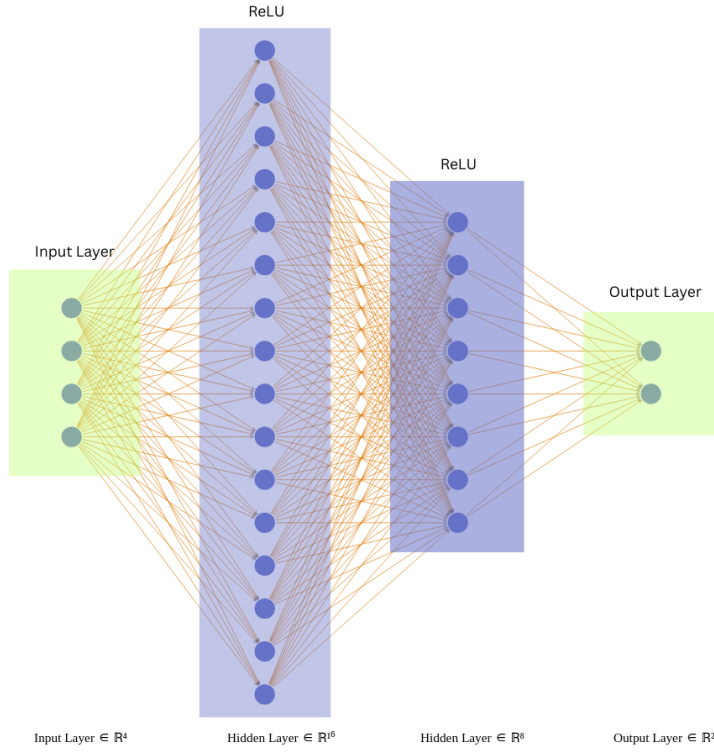


Figure 1. Feedforward Artificial Neural Network (ANN) architecture used for binary classification of blazar sources. The input layer accepts feature vectors of dimension 4 or 7, depending on the dataset. The network consists of three fully connected layers: the first maps the input to a 16-dimensional space, followed by a ReLU activation; the second compresses this to 8 dimensions with another ReLU activation; and the final layer maps to a 2-dimensional output representing the target classes (BL Lac and FSRQ). The model is trained using the AdamW optimizer with weight decay, a StepLR scheduler, and Cross-Entropy Loss.

other BCUs with complete data. However, many BCUs in the catalogs lack one or more key measurements, such as optical spectra, redshift, or X-ray flux. In such cases, the model cannot be used for classification tasks. Consequently, while the training procedure is general, the practical applicability of the model depends on the availability of the full set of required features.

After applying the required four-parameter filter to Dataset 1, we obtained a total of 1,499 sources classified as either *BL Lac* or *Flat Spectrum Radio Quasars (FSRQs)*. Of these, 809 were identified as *BL Lac* objects and 690 as *FSRQ*. The dataset was subsequently partitioned into an 80–20% train–test split, resulting in 1,199 samples used for training and the remaining 300 reserved for testing.

Applying an analogous filtering procedure to Dataset 2, incorporating the three additional parameters, yielded 988 sources in total, of which 567 classified as *BL Lac* and 421 as *FSRQs*. As with Dataset 1, an 80–20% split was adopted, allocating 790 samples for training the ANN model and 198 for testing.

Additionally, we created a separate PyTorch dataset comprising sources labelled as “Blazar Uncertain Type” (BCU), from both Dataset 1 and 2, which were held out as unlabelled data for prediction. For Dataset 1, we obtained 110 BCU events, and for Dataset 2, we obtained 82 events, in total.

The results of our ANN model on the test data are shown in Figure 2a for Dataset 1, trained on four features, and in Figure 2b for Dataset 2, trained with the inclusion of three additional features. Both figures present the outcomes in the form of confusion matrices, where the true labels are shown along the y-axis and the ML-predicted labels along the x-axis. A reliable model is expected to produce most of its predictions along the diagonal blocks, indicating agreement between true and predicted classes.

For Dataset 1 (Figure 2a), the confusion matrix shows that the ANN achieves a strong and well-balanced classification performance using only the four basic features (radio flux, optical magnitude, X-ray flux, and redshift). The diagonal elements indicate that 91.3% of the true FSRQs are correctly identified as FSRQs, while 93.4% of the true BL Lacs are correctly classified. The off-diagonal entries remain below 10%, with only 8.7% of FSRQs misclassified as BL Lacs and 6.6% of BL Lacs predicted as FSRQs. This indicates that the model is able to separate the two blazar subclasses reasonably well using the limited feature set.

In contrast, Dataset 2 (Figure 2b), which incorporates three additional physical features, synchrotron peak frequency, spectral index, and power-law index gives a dif-

ferent output. The classification of BL Lacs is with 93.1% correct identification and a misclassification rate of only 6.9%. The FSRQ accuracy decreases slightly to 88.8%, accompanied by a higher confusion rate 11.2% toward the BL Lac class. This suggests that while the added spectral features should provide more discriminative power for identification, they may also introduce overlap or ambiguity in the feature space, which can be because the training sample size for Dataset 2 is smaller than that of Dataset 1. Overall, these matrices quantify how well the model distinguishes the two blazar subclasses.

The corresponding Receiver Operating Characteristics (ROC) curves for the two models are shown in Figure 3a (Dataset 1) and Figure 3b (Dataset 2). The ROC curve plots the True Positive Rate (TPR or sensitivity) against the False Positive Rate (FPR = 1 - specificity) across various classification thresholds, thereby providing a comprehensive picture of the trade-off between correctly identifying positive cases and incorrectly misclassifying negative ones. A model with no discriminative capability would yield a diagonal line (AUC = 0.5), whereas a perfect classifier would achieve a curve passing through the top-left corner (AUC = 1.0). The Area Under the Curve (AUC) serves as a quantitative measure of performance, with higher values indicating stronger discriminative ability. The Deep Learning structure has also been used in [B. M. O. Fraga et al. \(2021\)](#), where they identify the blazars from the parent population of AGN based on the broadband spectral energy distribution (SED). They have compiled the broadband SED from the public platform “Open Universe VOU-Blazars tool.” They achieve the accuracy of distinguishing blazars from other AGN of 98%. Their study does not attempt to classify the blazars into the subclasses. In addition to their main classification results, [B. M. O. Fraga et al. \(2021\)](#) carried out several robustness tests that are useful for comparing with our work. They examined how the model behaves when the amount of available data is limited by training on sparsely sampled SEDs (using only the least-populated 10 % of sources). Even in this case, the classifier maintained stable ROC–AUC and PR–AUC values across folds. They also repeated the training multiple times with different random splits of the data and found that the accuracy curves were very similar in each run, indicating that their results are not strongly affected by random initialization.

In our study, the incorporation of precision–recall (PR) curves together with a k-fold cross-validation framework serves a similar purpose to the validation strategy employed in their work. The PR curve is par-

ticularly informative for imbalanced classification problems, as it highlights the trade-off between precision (the proportion of predicted positives that are correct) and recall (the proportion of true positives successfully identified). This makes PR analysis especially suitable for evaluating the reliability of our classifier in identifying the minority class.

As illustrated in Figure 4, the PR curves for both Dataset 1 (Figure 4a) and Dataset 2 (Figure 4b) exhibit consistently high precision across nearly the entire recall range, with only a sharp decline near full recall. The narrow shaded regions representing the standard deviation across folds indicate minimal variability in model behavior under different training subsets. Combined with the stability observed in our ROC and PR curves, these results reinforce that our ANN demonstrates a strong degree of robustness and consistency, comparable to the level of reliability reported in their study.

To further validate that our model generalizes well to unseen data, we present the train and test loss curves in Figures 5a and 5b, corresponding to Dataset 1 and Dataset 2, respectively. In both cases, the training and testing losses decrease and converge, demonstrating that the model does not suffer from either overfitting or underfitting. However, we can see that in Figure 5b, which is the train-test loss curve on Dataset 2, we have more stable learning, and this can be attributed to more features as compared to Dataset 1.

To evaluate the performance of the proposed model, three standard classification metrics were used: *precision*, *recall*, and the *F1-score*. Precision quantifies the proportion of correctly identified positive samples among all predicted positive samples, thereby measuring the model’s ability to avoid false positives. Recall, on the other hand, measures the proportion of correctly identified positive samples among all actual positive samples, indicating how well the model captures true instances. The F1-score is the harmonic mean of precision and recall, providing a balanced measure that considers both false positives and false negatives. In addition, the overall *accuracy* of the classifier was computed to represent the percentage of correctly classified samples across both classes. We present these metrics for both datasets, in one of the folds, in the below subsections:

3.1. Performance on Dataset 1

For Dataset 1, the classifier was evaluated on distinguishing between Flat Spectrum Radio Quasars (FSRQs) and BL Lacertae objects (BL Lacs). The model achieved an overall accuracy of **92%**, demonstrating strong discriminatory power between the two source

types. As shown in Table 1, the precision, recall, and F1-score values were consistently high for both classes. Specifically, the FSRQ class achieved a precision, recall, and F1-score of **0.91** each, while the BL Lac class obtained slightly higher values of **0.92** across all three metrics. The balanced performance across both categories indicates that the model does not exhibit a significant bias toward either class and can reliably classify sources into their respective categories.

Table 1. Classification report for Dataset 1 (FSRQ vs BL Lac).

Class	Precision	Recall	F1-score	Support
FSRQ	0.91	0.91	0.91	142
BL Lac	0.92	0.92	0.92	158
Accuracy	0.92 (on 300 samples)			
Macro Avg	0.92	0.92	0.92	300
Weighted Avg	0.92	0.92	0.92	300

3.2. Performance on Dataset 2

For Dataset 2, the model was similarly tested on the task of distinguishing between FSRQs and BL Lacs. The classifier achieved an overall accuracy of **91%**, indicating strong generalization performance across the two source categories. As summarized in Table 2, the FSRQ class achieved a precision of **0.94**, recall of **0.85**, and F1-score of **0.89**, while the BL Lac class attained a precision of **0.89**, recall of **0.95**, and F1-score of **0.92**. These results suggest that the model tends to be slightly more conservative in identifying FSRQs, as reflected by the lower recall, while maintaining high precision for both classes. Overall, the balanced macro- and weighted-average scores (**0.91**) confirm the model’s robustness and reliability in classifying blazar subclasses.

Table 2. Classification report for Dataset 2 (FSRQ vs BL Lac).

Class	Precision	Recall	F1-score	Support
FSRQ	0.94	0.85	0.89	89
BL Lac	0.89	0.95	0.92	109
Accuracy	0.91 (on 198 samples)			
Macro Avg	0.91	0.90	0.91	198
Weighted Avg	0.91	0.91	0.91	198

We saved models from each fold of the k-fold cross-validation step and made inferences on the BCUs from both datasets. We take the average of the probabilities, and thus, the predictions obtained from the trained

ANN models for BCUs in Datasets 1 and 2 are provided in Appendix A. Furthermore, a cross-comparison of the prediction outcomes from both models, based on the name of the events, revealed that 64 sources were consistently assigned to the same class, whereas 15 sources exhibited discrepancies, being classified differently by the two models.

4. CONCLUSION

In this study, we constructed and evaluated artificial neural network (ANN) models for the classification of blazars using multi-wavelength data drawn from several authoritative astronomical catalogues, including the Fermi-LAT 4FGL-DR3, ROMA-BZCAT v5, and the 3LAC dataset. Blazars have characteristic features across different regions of the EM spectrum and thus we exploit that knowledge to build our analysis pipeline such that we take into account features from all those different parts of the spectrum.

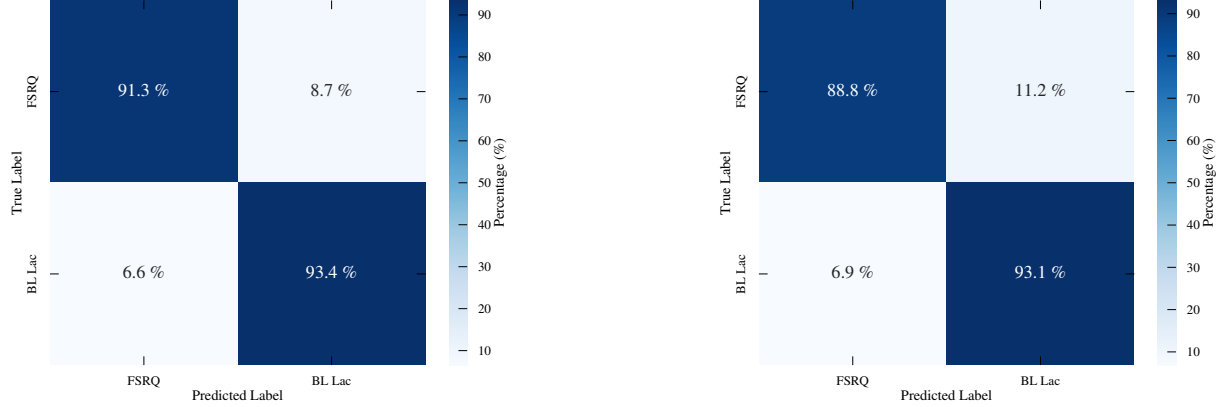
Our classification pipeline, implemented in PyTorch, demonstrated that even a relatively simple feed-forward ANN can effectively distinguish between BL Lac objects and FSRQs using features spanning radio, optical, X-ray, and gamma-ray bands. The inclusion of additional astrophysical parameters, such as synchrotron peak frequency and spectral index, in Dataset 2 led to a stable learning and equally good classification performance, as evidenced by the loss curves and confusion matrices. These results underscore the importance of incorporating physically meaningful features that reflect the underlying emission mechanisms of blazars.

The training and test loss curves for both datasets indicate stable learning behaviour without signs of overfitting or underfitting. However, to further enhance model convergence and generalization, future work could incorporate feature engineering, which might lead to more stable learning.

As compared to [A. Agarwal \(2023\)](#) we can see that they achieve a combined AUC score of ~ 0.964 which is comparable to our model achieving an AUC score of ~ 0.977 . Also F1 score is comparable with that of [G. Bhatta et al. \(2024\)](#) highlighting strong confidence in our model.

Overall, this work highlights the potential of machine learning approaches in astrophysical classification tasks and provides a scalable framework for future studies involving larger and more diverse datasets. In addition, our results show that the model's applicability depends on the completeness of multi-wavelength features available for each source. While the ANN was trained using radio flux, optical magnitude, X-ray flux, redshift, and additional spectral features (Dataset 2),

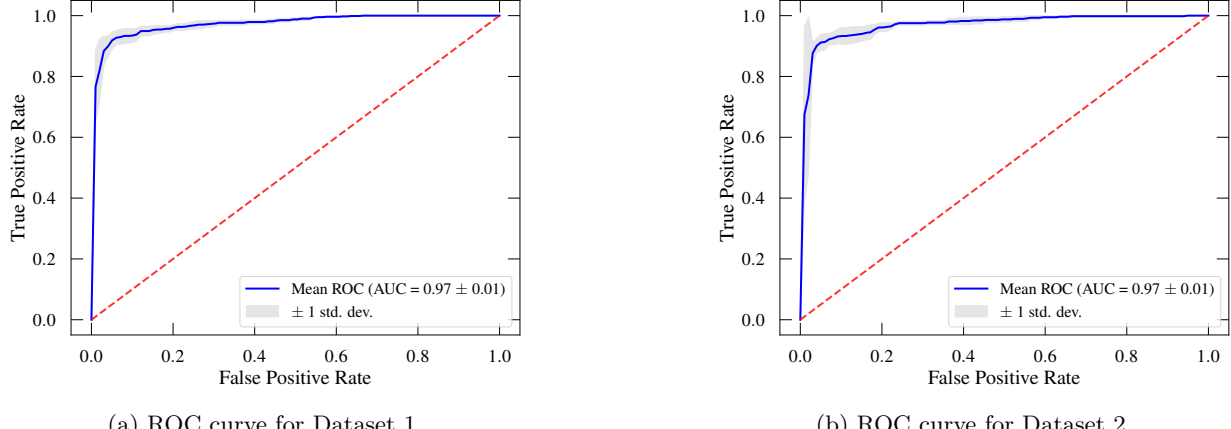
many BCUs in current catalogs still lack optical or X-ray measurements, which limits direct classification for these sources. As future Fermi releases and upcoming surveys provide more complete datasets, this approach can be scaled to classify a significantly larger BCU population, ultimately improving catalog completeness and contributing to broader studies of jet physics, population statistics, and next-generation facilities such as the Cherenkov Telescope Array (CTA). Moreover, our ANN approach is flexible and can easily incorporate new multi-wavelength data as they become available. By helping to identify uncertain blazar candidates more reliably, it opens the door for targeted follow-up observations and a deeper understanding of blazar populations and jet physics. While the model performs well overall, its accuracy is naturally limited for sources with missing key features, highlighting the continued importance of comprehensive datasets and future surveys. Furthermore, future efforts could benefit from incorporating interpretability tools such as SHAP values or feature-importance analysis. These techniques would help identify which physical parameters—such as synchrotron peak frequency, optical magnitude, or X-ray flux; play the most influential role in the BL Lac versus FSRQ separation. Such insights would not only enhance the transparency of the ANN's decision-making process but also strengthen the connection between the machine-learning results and the underlying jet physics.



(a) Dataset 1: Confusion matrix based on radio flux, optical magnitude, X-ray flux, and redshift.

(b) Dataset 2: Confusion matrix with additional features such as synchrotron peak frequency, spectral index, and power-law index.

Figure 2. Comparison of confusion matrices showing classification performance for the two datasets. Subfigure (a) shows the confusion matrix plot for Dataset 1, and Subfigure (b) presents the confusion matrix plot for Dataset 2.



(a) ROC curve for Dataset 1.

(b) ROC curve for Dataset 2.

Figure 3. Receiver Operating Characteristic (ROC) curves illustrating the performance of the classification model on two independent datasets. Subfigure (a) shows the ROC curve for Dataset 1, and Subfigure (b) presents the ROC curve for Dataset 2, allowing direct comparison of model effectiveness across different datasets.

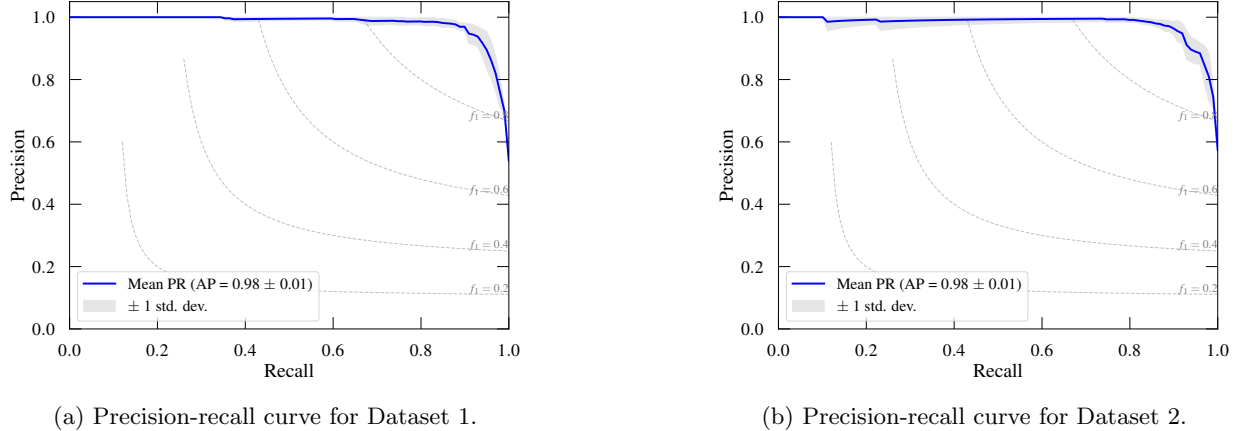


Figure 4. Precision-recall (PR) curves illustrating the performance of the classification model on two independent datasets. Subfigure (a) shows the PR curve for Dataset 1, and Subfigure (b) presents the (PR) curve for Dataset 2, allowing direct comparison of model effectiveness across different datasets.

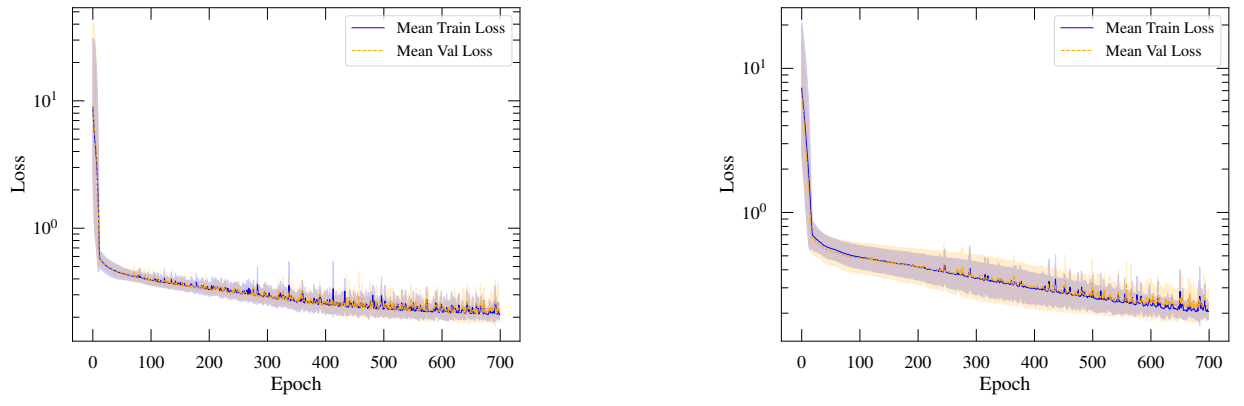


Figure 5. Loss curve comparison indicating the convergence behaviour for the two datasets.

ACKNOWLEDGMENTS

We acknowledge the respective groups or collaborations for developing the FERMI-LAT catalogue, ROMA-BZCAT catalogue, and LAT AGN catalogue.

DATA AVAILABILITY

All multi-wavelength parameters used to train the ANN models in this work are publicly available from the astronomical catalogues referenced in the text, including ROMA-BZCAT, Fermi-LAT 4FGL-DR4, and the 3LAC release. The full codebase used for data pre-

processing, model training, and evaluation is openly accessible at our GitHub repository: https://github.com/AfrozSaqlain/Light_Curve_of_BlaZars_ML.

Facilities: All the data analysis and ML training were performed on a laptop with NVIDIA RTX 4070 and Intel Core i7 processor, with 32 GB of RAM.

Software: PyTorch [A. Paszke et al. \(2019\)](#), Scikit-learn [F. Pedregosa et al. \(2018\)](#), TOPCAT [M. Taylor \(2017\)](#)

APPENDIX

A. PREDICTION MADE ON BCUS

Source Name	FR	Rmag	FX	z	Predicted Label
5BZU J0023+4456	140.0	21.7	0.00	2.023	FSRQ
5BZU J0040+4050	47.0	19.9	1.05	0.000	BL Lac
5BZU J0049-4457	206.0	15.8	2.31	0.121	BL Lac
5BZU J0058+3311	161.0	20.9	0.00	1.369	FSRQ
5BZU J0058-5659	485.0	17.4	1.38	0.000	BL Lac
5BZU J0100+0745	99.0	21.3	0.00	0.000	BL Lac
5BZU J0102+5824	849.0	19.0	0.79	0.644	FSRQ
5BZU J0110+6805	1715.0	16.5	0.28	0.000	BL Lac
5BZU J0128+4439	40.0	20.3	0.00	0.228	BL Lac
5BZU J0133-5200	352.0	17.8	0.88	0.000	BL Lac
5BZU J0204+1514	4068.0	22.0	0.02	0.833	FSRQ

Table 3. Predicted labels for Blazar Candidate of Uncertain type (BCU) sources obtained using the ANN model trained on Dataset 1 (with four features).

The complete table of predicted classes for BCUs is given at the following link, for both datasets 1 and 2: https://github.com/AfrozSaqlain/Light_Curve_of_BlaZars_ML/tree/main/data.

Source Name	FR	Rmag	FX	z	Log ν Sync Z corr. (Hz)	Power Law Index	Spectral Index	Predicted Label
5BZU J0023+4456	140.0	21.7	0.00	2.023	13.050	2.57	2.5685	FSRQ
5BZU J0040+4050	47.0	19.9	1.05	0.000	0.000	1.13	1.1323	BL Lac
5BZU J0049-4457	206.0	15.8	2.31	0.121	13.870	2.53	2.5279	FSRQ
5BZU J0058+3311	161.0	20.9	0.00	1.369	13.310	2.41	2.4073	FSRQ
5BZU J0058-5659	485.0	17.4	1.38	0.000	12.778	2.62	2.6164	FSRQ
5BZU J0100+0745	99.0	21.3	0.00	0.000	13.358	1.80	1.7966	BL Lac
5BZU J0102+5824	849.0	19.0	0.79	0.644	12.941	2.25	2.0943	FSRQ
5BZU J0110+6805	1715.0	16.5	0.28	0.000	14.864	1.99	1.9909	FSRQ
5BZU J0128+4439	40.0	20.3	0.00	0.228	13.969	2.33	2.3320	BL Lac
5BZU J0133-5200	352.0	17.8	0.88	0.000	12.063	2.63	2.6276	FSRQ
5BZU J0204+1514	4068.0	22.0	0.02	0.833	12.708	2.53	2.5301	FSRQ

Table 4. Predicted labels for Blazar Candidate of Uncertain type (BCU) sources obtained using the ANN model trained on Dataset 2 (with extended features including synchrotron peak frequency, power-law index, and spectral index).

REFERENCES

Ackermann, M., et al. 2015, *Astrophys. J.*, 810, 14, doi: [10.1088/0004-637X/810/1/14](https://doi.org/10.1088/0004-637X/810/1/14)

Agarwal, A. 2023, *Astrophys. J.*, 946, 109, doi: [10.3847/1538-4357/acbdfa](https://doi.org/10.3847/1538-4357/acbdfa)

Ballet, J., Bruel, P., Burnett, T. H., & Lott, B. 2023, <https://arxiv.org/abs/2307.12546>

Bhatta, G., Gharat, S., Borthakur, A., & Kumar, A. 2024, *Mon. Not. Roy. Astron. Soc.*, 528, 976, doi: [10.1093/mnras/stae028](https://doi.org/10.1093/mnras/stae028)

Butter, A., Finke, T., Keil, F., Krämer, M., & Manconi, S. 2022, *JCAP*, 04, 023, doi: [10.1088/1475-7516/2022/04/023](https://doi.org/10.1088/1475-7516/2022/04/023)

de Menezes, R., D'Abrusco, R., Massaro, F., Gasparini, D., & Nemmen, R. 2020, *ApJS*, 248, 23, doi: [10.3847/1538-4365/ab8c4e](https://doi.org/10.3847/1538-4365/ab8c4e)

Fossati, G., Maraschi, L., Celotti, A., Comastri, A., & Ghisellini, G. 1998, *MNRAS*, 299, 433, doi: [10.1046/j.1365-8711.1998.01828.x](https://doi.org/10.1046/j.1365-8711.1998.01828.x)

Fraga, B. M. O., Barres de Almeida, U., Bom, C. R., et al. 2021, *MNRAS*, 505, 1268, doi: [10.1093/mnras/stab1349](https://doi.org/10.1093/mnras/stab1349)

Gharat, S., Borthakur, A., & Bhatta, G. 2024, <https://arxiv.org/abs/2406.03782>

Gorriz, J. M., Clemente, R. M., Segovia, F., et al. 2024, Is K-fold cross validation the best model selection method for Machine Learning? <https://arxiv.org/abs/2401.16407>

Kang, S.-J., Li, E., Ou, W., et al. 2019, doi: [10.3847/1538-4357/ab558b](https://doi.org/10.3847/1538-4357/ab558b)

Kaur, A., Falcone, A. D., Stroh, M. D., Kennea, J. A., & Ferrara, E. C. 2019, *ApJ*, 887, 18, doi: [10.3847/1538-4357/ab4ceb](https://doi.org/10.3847/1538-4357/ab4ceb)

Kingma, D. P., & Ba, J. 2017, Adam: A Method for Stochastic Optimization, <https://arxiv.org/abs/1412.6980>

Kovačević, M., Chiaro, G., Cutini, S., & Tosti, G. 2020, *Mon. Not. Roy. Astron. Soc.*, 493, 1926, doi: [10.1093/mnras/staa394](https://doi.org/10.1093/mnras/staa394)

Mao, A., Mohri, M., & Zhong, Y. 2023, Cross-Entropy Loss Functions: Theoretical Analysis and Applications, <https://arxiv.org/abs/2304.07288>

Massaro, E., Maselli, A., Leto, C., et al. 2015, *Astrophys. Space Sci.*, 357, 75, doi: [10.1007/s10509-015-2254-2](https://doi.org/10.1007/s10509-015-2254-2)

Paszke, A., Gross, S., Massa, F., et al. 2019, PyTorch: An Imperative Style, High-Performance Deep Learning Library, <https://arxiv.org/abs/1912.01703>

Pedregosa, F., Varoquaux, G., Gramfort, A., et al. 2018, Scikit-learn: Machine Learning in Python, <https://arxiv.org/abs/1201.0490>

Taylor, M. 2017, *Informatics*, 4, 18, doi: [10.3390/informatics4030018](https://doi.org/10.3390/informatics4030018)